AGU PUBLICATIONS

JGR

Journal of Geophysical Research: Planets

RESEARCH ARTICLE
10.1002/2015JE004851

Key Points:
- Fractured rock masses can accommodate substantial strain prior to faulting
- Amount of global contraction is higher than from mapping alone
- Prefaulting strain requires an onset of contraction much earlier than observed

Correspondence to:
C. Klimczak,
klimczak@uga.edu

Citation:
Klimczak, C. (2015), Limits on the brittle strength of planetary lithospheres undergoing global contraction, *J. Geophys. Res. Planets, 120*, 2135–2151, doi:10.1002/2015JE004851.

Received 8 MAY 2015
Accepted 27 OCT 2015
Accepted article online 30 OCT 2015
Published online 10 DEC 2105

Limits on the brittle strength of planetary lithospheres undergoing global contraction

Christian Klimczak[1]

[1]Structural Geology and Geomechanics Group, Department of Geology, University of Georgia, Athens, Georgia, USA

Abstract The degree and depth of fracturing of the lithospheres of Mars, Mercury, and the Moon remain poorly known. It is these two properties, however, that govern the mechanical behavior of a planetary lithosphere. Considering the lithosphere as a cohesive rock mass that consists of small and large blocky, interlocked rock fragments, as opposed to an intact body or a body entirely lacking cohesion, provides insight into the effect of lithospheric fracturing on tectonic processes on these bodies. Characterization of the near-surface lithospheric brittle strength that incorporates the degree of fracturing is necessary for a realistic assessment of the lithospheric response to global contraction resulting from interior secular cooling. Such an assessment shows that all of these bodies could have accommodated substantial amounts of global contraction prior to the formation of thrust fault-related landforms. In fact, their lithospheres were sufficiently strong so as to experience changes in radius of as much as 2.2 ± 0.4 km (Mars), 2.1 ± 0.4 km (Mercury), and 1.4 ± 0.3 km (the Moon) prior to the onset of widespread thrust faulting. These values imply that the process of global contraction begins before any evidence of it is established in the geologic record, requiring an earlier onset, and for Mars and Mercury a faster initial strain rate, of global contraction than previously thought. Such results add a heretofore unrecognized component of planetary radial decrease with implications for timing and strain rate to studies of global contraction on Mars, Mercury, and the Moon, in particular, and to planetary bodies, in general.

1. Introduction

Fractures are planar structural heterogeneities whose opposing surfaces are displaced relative to one another, irrespective of the mode of displacement or mechanics of formation [e.g., *Schultz and Fossen*, 2008]. Not only do fractures represent lithospheric discontinuities that may be utilized as planes of weakness along which tectonic activity is accommodated or volcanic intrusive activity or fluid migration is facilitated, but they are also crucial for understanding and characterizing the overall strength of planetary lithospheres and the conditions for rock failure [*Schultz*, 1993]. Hence, the degree and depth of fracturing of planetary lithospheres are important factors for assessing the tectonic and near-surface geophysical evolution of solid bodies in the Solar System.

The extent to which a planetary lithosphere is fractured is poorly constrained, but it is clear that on planetary scales no rock unit has remained intact over geologic time, at least for near-surface conditions. On Earth, fractures are ubiquitous in rock units at the outcrop or larger scales. Natural fractures and fracture zones are commonly found in deep boreholes [e.g., *Seeburger and Zoback*, 1982; *Lin et al.*, 2007], and although fracture connectivity and apertures generally decrease with depth [e.g., *Snow*, 1968], wide fracture zones have been identified at depths down to 9 km [*Emmermann and Lauterjung*, 1997].

Planetary surfaces are heavily modified by impacts, which damage lithospheres [*Melosh*, 1984; *Ahrens and Rubin*, 1993; *Xia and Ahrens*, 2001; *Collins et al.*, 2004] and so introduce a multitude of fractures at even greater lithospheric depths. Over geologic time, therefore, continuous impact bombardment heavily damages the uppermost few kilometers of a planetary lithosphere, producing multifaceted, angular, interlocked blocks of material of different sizes formed by more or less randomly oriented sets of fractures, with the degree of fracturing decreasing with depth. On the Moon, for example, the crustal seismic wave velocity structure obtained from the Apollo seismic experiment is consistent with fractured dry rock to a depth of 20 km, with fracturing interpreted to be induced by shock effects of impacts [*Dainty et al.*, 1974; *Toksöz et al.*, 1974]. Furthermore, analysis of high-resolution gravity data returned by the Gravity Recovery and Interior Laboratory mission revealed that the porosity of the lunar crust is much higher than previously thought [*Wieczorek et al.*, 2013]. Porosity variations resolved within and around impact basins are consistent with

the impact cratering process [*Wieczorek et al.*, 2013], highlighting the influence of impact bombardment on the fracturing of the lithosphere of the Moon and likely those of the other terrestrial planets.

Fractured, heterogeneous volumes of rock, irrespective of scale, degree of fracturing, and quality of the fractures, are referred to as rock masses. Their classification, when used in conjunction with observations and models, are powerful aids for relating rock conditions at one site to conditions encountered at others [*Bieniawski*, 1989]. Relating established conditions of rock masses on Earth to the lithospheres of other solid planetary bodies could thus provide a better understanding of lithospheric deformation and other near-surface geophysical processes on solid-surface bodies in general.

Commonly used rock mass classification schemes include the Geomechanics Classification or Rock Mass Rating system (RMR) [*Bieniawski*, 1989], as well as the closely related Geologic Strength Index (GSI) [*Hoek*, 1994; *Marinos and Hoek*, 2000]. The RMR and GSI classification schemes allow the degree of fracturing and conditions of weaknesses within a rock mass to be related to its strength [e.g., *Hoek et al.*, 1992; *Hoek*, 1994] and elastic moduli [e.g., *Serafim and Pereira*, 1983; *Hoek*, 1994]. Both schemes provide a quantitative basis for the degree of fracturing to be included in rock-mechanical characterizations on planetary scales, at which rock volumes can no longer be considered intact [*Schultz,* 1993, 1995, 1996]. RMR has previously been applied to a variety of topics in planetary geomechanics [*Schultz*, 1993; *Schultz et al.*, 2006; *Nahm and Schultz*, 2007; *Klimczak*, 2014; *Klimczak et al.*, 2015], but GSI has not found wide consideration in planetary geology yet. However, given the limitations of RMR when considering poor and very poor quality rock masses [*Hoek*, 1994], there is potential for the GSI scheme to be applied to strength characterizations of both heavily jointed near-surface rock masses as well as regolith and megaregolith materials [e.g., *Williams et al.*, 2013].

In addition to damage from impacts, the lithospheres of Mars, Mercury, and the Moon have also been deeply fractured by thrust faults [e.g., *Schultz and Watters*, 2001; *Watters et al.*, 2002; *Byrne et al.*, 2015]. The formation of, and strain accumulation along many planetary thrust faults are interpreted to be the result of global contraction, a process acting in response to the secular cooling of the planetary interior [e.g., *Solomon and Chaiken*, 1976]. Thermal models predict that the interiors of Mars, Mercury, and the Moon have cooled appreciably over geological time, and so each body must have contracted to some extent [*Solomon and Chaiken*, 1976; *Solomon,* 1977, 1986; *Schubert and Spohn*, 1990; *Zuber*, 2000; *Hauck and Phillips*, 2002; *Hauck et al.*, 2004; *Shearer*, 2006; *Andrews-Hanna et al.*, 2008; *Dombard and Hauck*, 2008; *Laneuville et al.*, 2013; *Michel et al.*, 2013; *Tosi et al.*, 2013; *Zhang et al.*, 2013]. For all three bodies, but for the Moon in particular, estimates of global contraction obtained from thrust fault mapping have disagreed with thermal evolution models, with observations suggesting planetary radius decreases [*Strom et al.*, 1975; *Watters et al.*, 1998; *Watters and Nimmo*, 2010; *Watters et al.*, 2009, 2010; *Nahm and Schultz*, 2011; *Di Achille et al.*, 2012] that are much smaller than model predictions [*Solomon*, 1977; *Dombard and Hauck*, 2008; *Laneuville et al.*, 2013; *Zhang et al.*, 2013]. Recent thrust fault analysis has revealed a much greater amount of contraction on Mercury than previously thought [*Byrne et al.*, 2014] and so provides a closer match to predictions from thermal modeling [e.g., *Tosi et al.*, 2013].

However, radius change estimates derived from thrust fault mapping alone do not account for lithospheric strength and that some portion of the compressive stresses imposed on a lithosphere by global contraction can be accommodated prior to the formation of thrust faults. It is therefore likely that an additional component of global contraction exists that has not previously been recognized. As rock mass strength depends on the degree of fracturing within a rock mass, a detailed rock mass characterization for conditions applicable to Mars, Mercury, and the Moon is therefore important for understanding the onset of thrust faulting and the lithospheric response to global contraction on these bodies.

2. Compressive Strength of a Planetary Lithosphere

Planetary lithospheres affected by continuous impact bombardment very likely contain various discontinuities, such as stratification of impact and volcanic rock units, pseudotachylitic zones, and fractures of all orientations. The fracturing causes a strength drop and so weakens the lithosphere. Such a lithosphere is likely in frictional failure equilibrium [e.g., *Zoback*, 2007], and faulting could utilize any preexisting discontinuity as

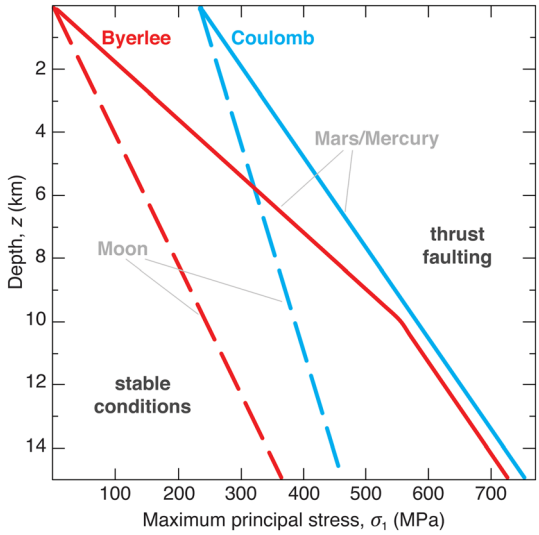

Figure 1. Byerlee and Coulomb strength envelopes (red and blue lines, respectively) for Mars and Mercury (solid lines), and for the Moon (dashed lines).

long as the frictional resistance to sliding is overcome [*Byerlee*, 1978]. The critical values of the principal stresses for frictional sliding in a dry lithosphere, regardless of its composition, can be obtained from Byerlee's intermediate- and high-pressure laws [*Brace and Kohlstedt*, 1980; *Kohlstedt and Mackwell*, 2010] as:

$$\begin{aligned} \sigma_1 &\cong 5\sigma_3 \quad \text{for} \quad \sigma_3 < 110 \ \text{MPa} \\ \sigma_1 &\cong 3.1\sigma_3 + 210 \ \text{MPa} \quad \text{for} \quad \sigma_3 > 110 \ \text{MPa}, \end{aligned} \tag{1}$$

where σ_1 and σ_3 are the greatest and least compressive principal stress components, respectively. In a tectonic regime dominated by global contraction, where the least compressive stress acts vertically and is equal to the overburden pressure (i.e., $\sigma_v = \sigma_3 = \rho g z$, where ρ is density, g is surface gravitational acceleration, and z is depth) and where the most compressive stresses act in the horizontal plane (i.e., $\sigma_H = \sigma_1$), widespread thrust faulting is predicted to occur [e.g., *Anderson*, 1951] once the stress values in equation (1) are reached (Figure 1).

The brittle strength envelopes for Mercury and Mars (Figure 1, red solid line), as well as for the Moon (Figure 1, red dashed line), for an assumed average lithospheric density of $\rho = 3000$ kg/m^3, describe the critical stresses for frictional slip in contractional tectonic regimes for Byerlee's law as a function of depth (z). Lithospheric strength increases with depth as it largely depends on the overburden. Mars and Mercury have a similar surface gravitational acceleration, g (Table 1), and so their strength envelopes are nearly identical. The lunar lithosphere is generally weaker than those of Mercury and Mars due to the lower g, and conditions for the high-pressure friction law are not satisfied in the upper 15 km (Figure 1). In contrast, the transition from the intermediate- to high-pressure law on Mars and Mercury occurs at ~10 km depth.

Byerlee's law assumes a pervasively fractured rock volume with fractures of all orientations [*Byerlee,* 1967a, 1967b]. The curves in Figure 1 show that the lithospheres are predicted to have no strength at the surface, which is consistent with rock masses having no cohesion. However, each of these planetary bodies possesses rock cliffs and slopes greatly exceeding the angle of repose for regolith material [*Carrier et al.*, 1991], as well as large-scale tectonic landforms, which together indicate that near-surface rock masses display some level of cohesion. The near-surface brittle strength of rock masses might therefore not be adequately described by Byerlee's law [*Schultz,* 1992a, 1992b, 1993].

Principal stresses in a dry lithosphere for the Coulomb criterion for frictional slip [*Jaeger et al.*, 2007, p. 92] are given as

$$\sigma_1 = \sigma_c + q\sigma_3, \tag{2}$$

Table 1. Physical Planetary Characteristics and Nominal Rock-Physical Parameters Used for the Analysis of Planetary Radius Change for Mars, Mercury, and the Moon Accommodated Prior to the Formation of Thrust Faults[a]

	R (km)	g (m/s^2)	ρ (kg/m^3)	C_0 (MPa)	μ	σ_c (MPa)	m_i	E (GPa)	ν	ΔR_i (km)	ΔR_{max} (km)	ΔR_{min} (km)
Mars	3390	3.71	3000	66	0.6	234	22	73	0.25	8.1–8.3	2.0–2.2	0.2–0.5
Mercury	2440	3.70	3000	66	0.6	234	22	73	0.25	5.9–6.0	1.9–2.1	0.4–0.6
Moon	1737	1.62	3000	66	0.6	234	22	73	0.25	4.2	1.4	0.3

[a] R = planetary radius, g = surface gravitational acceleration, ρ = rock density, C_0 = cohesion, μ = coefficient of friction, σ_c = unconfined compressive strength, m_i = Hoek-Brown parameter for intact rock, E = Young's modulus, ν = Poison's ratio, ΔR_i = Radius change derived for intact rock, ΔR_{max} = radius change derived for rock mass with upper bound of GSI values, and ΔR_{min} = Radius change derived for rock mass with lower bound of GSI values.

where σ_c is the uniaxial (or unconfined) compressive strength of the (intact) rock mass and q relates to the average coefficient of friction (μ) by $q = \left(\sqrt{\mu^2+1}+\mu\right)^2$. The unconfined compressive strength relates to the rock-specific parameters cohesion (C_0) and to μ by

$$\sigma_c = 2C_0\left(\sqrt{\mu^2+1}+\mu\right). \tag{3}$$

The brittle strength envelopes for tectonic regimes dominated by global contraction given by the Coulomb criterion on the Moon, Mars, and Mercury are shown as blue curves in Figure 1. These envelopes characterize the critical stresses on each of these bodies where the resistance to frictional sliding within a cohesive volume of rock is overcome and thrust faulting is initiated.

The Coulomb envelopes for Mars and Mercury (Figure 1, blue solid line) and the Moon (Figure 1, blue dashed line) are shown for lithospheres with an assumed density of $\rho = 3000$ kg/m^3, a coefficient of friction of $\mu = 0.6$, and a cohesion of $C_0 = 66$ MPa, values consistent with laboratory measurements of intact mafic igneous rocks [e.g., *Goodman*, 1989]. The near-surface strength of the lithosphere in these curves is dependent on the rock-specific unconfined compressive strength (i.e., $\sigma_3 = 0$ and so $\sigma_1 = \sigma_c$ directly at the surface), and so varies for different rock types. *Schultz* [1993, 1995] listed experimentally derived values for the unconfined compressive strength of basalts, the rock type most applicable to the lithospheres of Mercury, Mars, and to some extent also to the Moon, ranging between 81 and 479 MPa with a mean of $\sigma_c = 266$ MPa. This range of values is consistent with the calculated value of $\sigma_c = 234$ MPa (equation (3)) used here to derive the Coulomb strength envelopes in Figure 1. The near-surface brittle strength of rock masses might also not be adequately described by the Coulomb criterion using cohesion and hence unconfined compressive strength values of intact materials.

The Hoek-Brown failure criterion also takes rock mass cohesion into account, but additionally can incorporate various degrees of fracturing of rock masses by means of RMR [*Hoek and Brown,* 1980, 1988] or GSI [*Hoek*, 1994; *Hoek and Brown*, 1997; *Marinos and Hoek*, 2000]. Both the RMR and the GSI classification schemes rank the degree and conditions of fractures in a rock mass on a scale to 0 to 100, where intact rock is rated as 100, and disintegrated or very poor quality rock masses are assigned the lowest possible ratings of 8 (for RMR) [*Bieniawski*, 1976] or ≈ 7 (for GSI) [*Hoek and Brown*, 1997]. In the general form, the principal stresses at failure for the Hoek-Brown criterion were defined by *Hoek* [1994] as

$$\sigma_1 = \sigma_3 + \sigma_c\left(m\frac{\sigma_3}{\sigma_c}+s\right)^a, \tag{4}$$

where m, s, and a are empirically derived parameters describing rock mass strength characteristics. For RMR values greater than 25, these parameters relate to RMR [*Bieniawski*, 1989] by

$$m = m_i \exp\left(\frac{\mathrm{RMR}-100}{28}\right), \tag{5a}$$

$$s = \exp\left(\frac{\mathrm{RMR}-100}{9}\right), \tag{5b}$$

and

$$a = 0.5. \tag{5c}$$

The parameter m_i represents the initial value of m for intact rock that, for polymineralic igneous rocks such as basalts or anorthosites, was found to have a range of $17 \le m_i \le 33$ [e.g., *Hoek and Brown*, 1997].

The Hoek-Brown criterion as defined by equations (4) and (5a)–(5c) was found to be in good agreement for rock masses of reasonable quality [*Hoek*, 1994], where the rock strength is controlled by tightly interlocking angular blocks of rock. Such conditions are plausible for much of the brittle portions of the lithospheres of Mars, Mercury, and the Moon. However, for rock masses of low or no cohesion, i.e., regolith and megaregolith, the Hoek-Brown parameters describing rock mass strength characteristics are better related to GSI [*Hoek*, 1994] as

$$m = m_i \exp\left(\frac{\mathrm{GSI}-100}{28}\right), \tag{6a}$$

$$s = 0, \tag{6b}$$

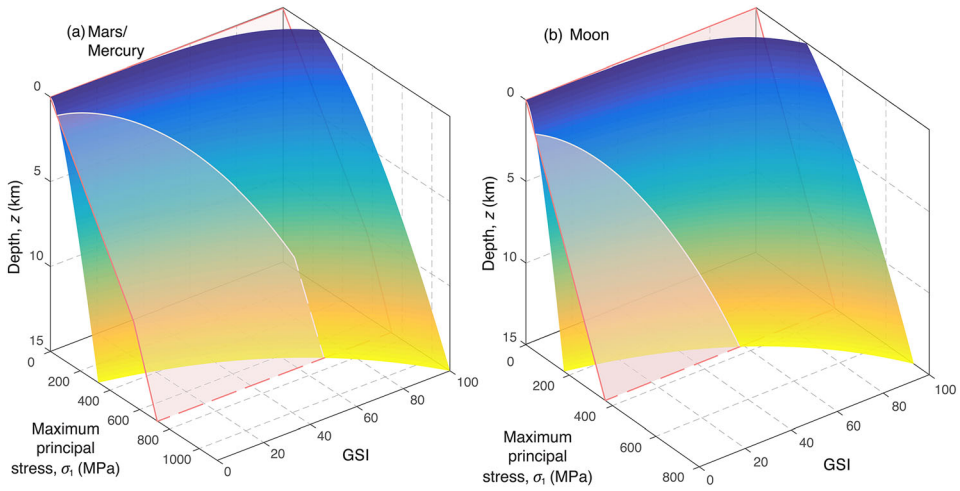

Figure 2. Variations of the Hoek-Brown failure envelopes with depths and degree of fracturing as measured by the Geologic Strength Index (GSI) with respect to Byerlee's law (light red transparent curves) for general comparison. Please note that only materials with no cohesion are adequately described by Byerlee's law and so the representative strength envelope is only truly valid for GSI ratings of zero. (a) Hoek-Brown and Byerlee envelopes for Mars and Mercury. (b) Hoek-Brown and Byerlee envelopes for the Moon.

and

$$a = 0.65 - \frac{\mathrm{GSI}}{200}. \tag{6c}$$

The Hoek-Brown criterion as defined by equations (4) and (6a)–(6c) is only appropriate for GSI < 25, and rock strength characterizations for greater GSI values follow the same relationships as outlined for RMR in equations (5a)–(5c) [*Hoek and Brown*, 1997].

The three-dimensional lithospheric strength envelopes for Mercury and Mars (Figure 2a) and the Moon (Figure 2b) for the combined classical (equations (4) and (5a)–(5c), for GSI > 25) and modified Hoek-Brown criteria (equations (4) and (6a)–(6c), for GSI < 25) illustrate the horizontal stress in a tectonic regime dominated by global contraction that must be reached for thrust faults to form. The strength envelopes are shown for the full range of possible degrees of fracturing (i.e., $7 \leq \mathrm{GSI} \leq 100$) as a function of depth. As with the strength envelopes for Byerlee's law and the Coulomb criterion (Figure 1), the curves for the Hoek-Brown criterion are shown for lithospheres with a density of $\rho = 3000$ kg/m^3, as well as a coefficient of friction of $\mu = 0.6$, and an initial cohesion for intact rock of $C_0 = 66$ MPa to derive the unconfined compressive strength (equation (3)). In addition, a value of m_i that is consistent with mafic, polycrystalline rock of 22 was chosen (Table 1) [*Hoek and Brown*, 1997]. The curves are shown in comparison with Byerlee's law (Figure 2, light red transparent curves).

The three-dimensional Hoek-Brown envelopes indicate that rock masses of reasonable to good quality at and near the surface (i.e., unconfined conditions) show an increase in compressive strength with increasing GSI and so they are able to resist some amount of applied stress prior to a faulting event. The unconfined compressive strength decreases with GSI but even for rock masses with high degrees of fracturing (e.g., GSI < 45) some strength remains at or near the surface. The near-surface strength of disintegrated, poorly interlocked blocks of rock and highly disturbed rock masses predicted with the modified Hoek-Brown criterion (e.g., GSI < 25) is reduced due to a decrease of rock mass cohesion (Figure 2). Hence, the strength of megaregolith materials at the near-surface of terrestrial bodies may be best assessed with the GSI scheme and the modified Hoek-Brown criterion (equations (4) and (6a)–(6c); see section 3 for the GSI assessment of megaregolith materials).

Given that the Hoek-Brown criterion allows the degree of fracturing to be included, and so accounts for various levels of cohesion and avoiding lithospheric properties for end-member cases of either intact materials or materials entirely lacking cohesion, it is considered the most appropriate criterion for the characterization of lithospheric strength at and near planetary surfaces in this paper.

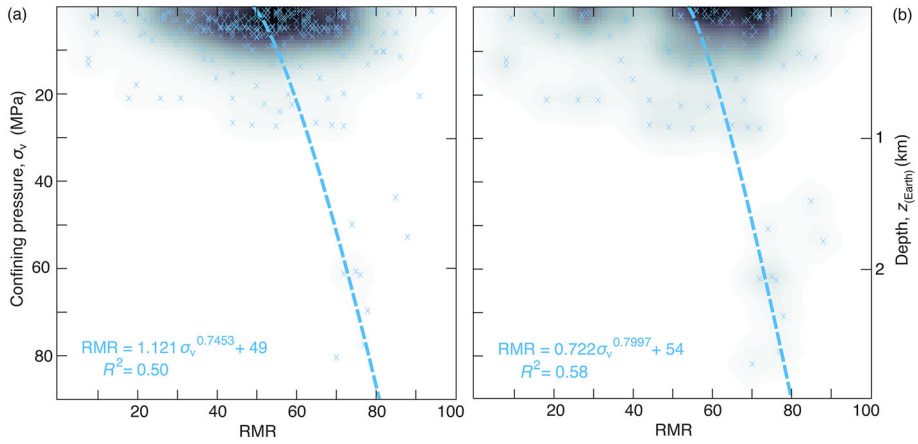

Figure 3. Depth distribution and density of the Rock Mass Rating (RMR) case history data with best fit power law curves. (a) Depth distribution and density of all 350 RMR values, including sedimentary, metamorphic, and igneous rocks appropriate for Mars. (b) Depth distribution and density of a subset of 113 RMR values including only massive polycrystalline rocks appropriate for Mercury and the Moon. The best fit power law functions for the entire data and the subset of data are within the 95% confidence bounds of one another.

3. Depth and Degree of Fracturing of Planetary Lithospheres

It is very likely that the brittle strength of a planetary lithosphere is wholly characterized neither by the mechanical properties of completely intact nor by entirely cohesionless materials but instead by the properties of a cohesive rock mass consisting of small and large blocky, interlocked rock fragments. Therefore, it is worth qualitatively characterizing the depth and degree of fracturing within planetary lithospheres—despite the many unknowns and limitations to quantify these properties—to assess better the strength of planetary lithospheres and their response to stresses in the brittle regime.

A set of 350 RMR case histories for tunneling and underground mining recorded for depths down to 2750 m provides first-order insight into the variability of RMR as a function of depth for different rock types on Earth [*Bieniawski*, 1989, p. 205–219]. The individual ratings (Figure 3, blue crosses), as well as the measurement density (Figure 3, light to dark gradient), are shown as a function of confining pressure (σ_v) and for the recorded depth range (z) for all available case histories (Figure 3a, $n = 350$) as well as for a subset of case histories comprising only massive, polycrystalline rock types (Figure 3b, $n = 113$). From the density cloud of the entire data set, where lighter and darker colors represent a lower and greater density of measurements, respectively, it is clear that most measurements were taken within the uppermost 300 m of the Earth's lithosphere; the greatest number of measurements return RMR values of 35–75 (Figure 3a). The full set of ratings encompasses a variety of different rock types, including sedimentary and metamorphic rocks that may be found on Mars but that may not occur on Mercury and the Moon. A previous study assigned the Burns Formation, a sedimentary sequence in Meridiani Planum, Mars, a RMR rating for dry conditions of 63 [*Nahm and Schultz*, 2007], which compares well to the densest scatter of RMR values on Earth analyzed in this study (Figure 3a).

The density cloud for polycrystalline rocks that are more likely representative for materials on Mercury and the Moon indicates that the majority of RMR values for such lithologies occur between 50 and 80 (Figure 3b). As no direct observations or other classifications currently exist, this range of RMR values is taken here as appropriate for the near-surface degree of fracturing for conditions present on Mercury and the Moon. It compares well to the established bounds for basaltic rock masses on Venus [*Schultz*, 1993].

RMR values at greater depths, i.e., deeper than 1 km, do not fall below 70, which is consistent with the expectation that the degree of fracturing generally decreases with increasing depth (Figure 3). A curve was fitted to the data (both complete and subset) to obtain an overview of the relationship between the degree of fracturing and depth. Best fits were achieved with power law functions, where the degree of fracturing as indicated by RMR was found to relate to confining pressure (in MPa), by

$$\mathrm{RMR} = 1.121\sigma_v^{0.7453} + 49 \quad \left(R^2 = 0.50\right) \tag{7a}$$

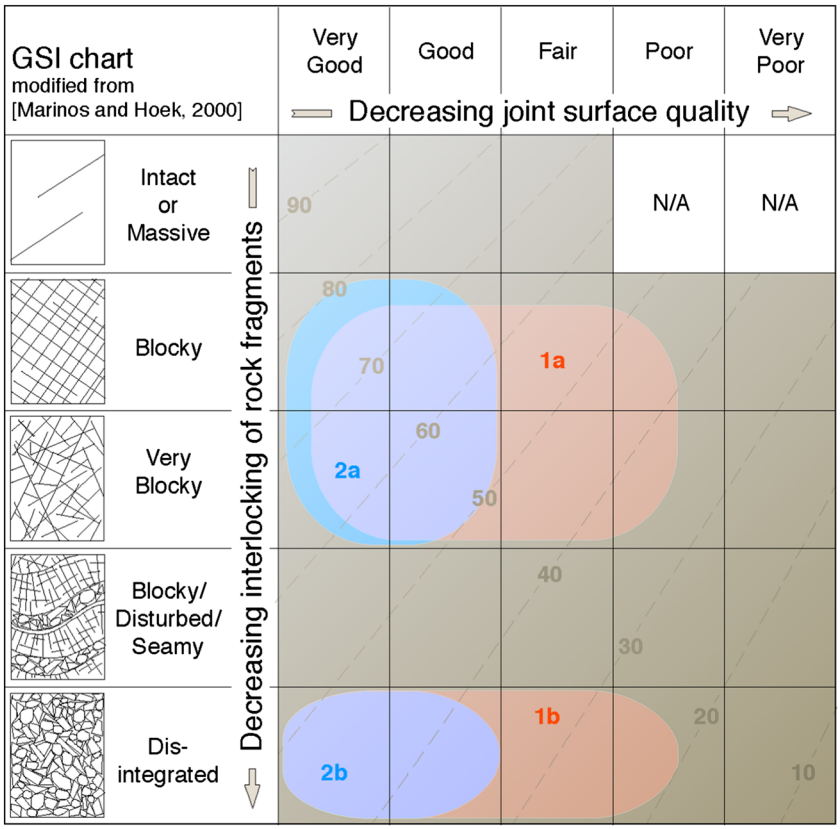

Figure 4. GSI estimation chart modified from *Marinos and Hoek* [2000]. Assessments for rock fragmentation and joint surface qualities in the lithosphere of Mars (shaded in red) show a range of GSI values of 35–75 for a cohesive rock mass (1a) and 20–50 for regolith materials (1b). Likely conditions for rock fragmentation and joint surface qualities for Mercury and the Moon (shaded in blue) show a GSI range of 50–80 for a cohesive rock mass (2a) and 35–50 for a regolith and megaregolith (2b).

and

$$\mathrm{RMR} = 0.722\sigma_v^{0.7998} + 54 \quad \left(R^2 = 0.58\right), \tag{7b}$$

with both curves being within the 95% confidence bounds of one another. Best fit RMR values directly at the surface (i.e., $\sigma_v = 0$) for these curves are predicted to be 49 and 54, respectively, consistent with the dense data scatter of RMR case histories at and near the surface.

The RMR values of the case histories are from studies between 1973 and 1987, making use of Bieniawski's Geomechanics Classification established prior to 1989 [e.g., *Bieniawski,* 1973, 1976]. *Bieniawski*'s [1976] RMR classification (termed here as RMR_{76}) was found to directly equate to the GSI classification scheme for ratings of $\mathrm{RMR}_{76} > 18$ [*Hoek*, 1994]. As the relationships given in equations (7a) and (7b) have their RMR_{76} minima at 49 or 54 and were derived from a data set with the vast majority of data points above $\mathrm{RMR}_{76} = 18$, these curves are equally applicable to the GSI scheme.

Further, the degrees of fracturing at and near the surface inferred from the case histories using the RMR ranges taken as applicable to Mars ($35 < \mathrm{RMR} < 75$) and Mercury and the Moon ($50 < \mathrm{RMR} < 80$) are also consistent with the GSI estimation chart (Figure 4). In this matrix chart, the GSI value is estimated by a qualitative assessment of the degree of rock fragmentation and the quality of the fracture surface conditions. The degree of rock fragmentation includes the number and orientation of different sets of discontinuities as well as the shape and degree of interlocking of the blocks that are separated by these discontinuities. The fracture surface quality includes the roughness of the fracture surface, as well as weathering and alterations on that surface and whether the fractures are filled or if their surfaces are coated with secondary minerals (for details see *Marinos and Hoek* [2000]).

Surface rock masses on Mars, as photographed by rovers, show a high degree of jointing. This physical appearance is consistent with "blocky" to "very blocky" conditions as defined by *Marinos and Hoek* [2000] as interlocked, partially disturbed rock with multifaceted, angular blocks formed by more than four joint sets that were likely introduced by impacts. Rover data also reveal the presence of alterations and veins [e.g., *Haskin et al.*, 2005], indicating that the quality of the fracture surfaces might range from "very good" to "fair" including both fresh, unweathered surfaces as well as moderately weathered and altered surfaces. Weathering-induced weakening of basalts in the Columbia Hills region on Mars was inferred by variations in the power consumption of the Rock Abrasion Tool (RAT) aboard the Mars Exploration Rover (MER) Spirit [*Thomson et al.*, 2013]. A range of GSI values for the Martian lithosphere of $35 < \mathrm{GSI} < 75$, similar to rock masses on Earth (Figure 3a), is therefore likely (Figure 4, region 1a). On that basis, a disintegrated, poorly interlocked, and heavily broken rock mass with a mixture of angular and rounded rock pieces, such as a Martian soil or regolith, would be classified with values of $20 < \mathrm{GSI} < 50$ (Figure 4, region 1b).

Rock masses at the near-surface of Mercury and the Moon can likely be classified as "blocky" to "very blocky," as multiple sets of fractures formed from the heavy impact bombardment on these bodies. Unlike Earth and Mars, the surfaces of these fractures are not affected by weathering or alteration and so they should be classified as "very good" to "good." A range of GSI values for the lithosphere of Mercury and the Moon between $50 < \mathrm{GSI} < 80$, as found for rock masses consisting of massive, polycrystalline rocks on Earth (Figure 3b), is therefore appropriate (Figure 4, region 2a). A disintegrated, poorly interlocked, heavily broken rock mass with a mixture of angular and rounded rock pieces, such as the regolith or mega regolith, would be assigned GSI values of 35–50 (Figure 4, region 2b).

The best fit curves described by equations (7a) and (7b) predict that conditions for an intact rock mass (i.e., RMR = 100) are reached at confining pressures of around 160 or 180 MPa. Given the large data scatter and the fair values for the goodness-of-fit analysis with the best fit curves (equations (7a) and (7b) and Figure 3), some uncertainties exist for these depth values and so they should only be regarded as first-order estimates. Nevertheless, confining pressures of that order are reached on Earth at around 6 km depth, at 15–16 km depth on Mars and Mercury, and at depths of 34–37 km on the Moon. Under the assumption that the increase of RMR with depth (equations (7a) and (7b)) is as applicable to Mars, Mercury, and the Moon as it is for Earth, and given the agreement of near-surface RMR values on Earth and Mars (Figures 3 and 4), it is likely that the lithospheres of these planetary bodies are substantially fractured and do not exist as intact rock until depths of around 15 km (Mars and Mercury) to 35 km (Moon). These lunar values are somewhat greater than, but largely agree with, previous findings from the Apollo seismic experiment of 20–25 km [*Dainty et al.*, 1974; *Toksöz et al.*, 1974].

4. Application to Global Contraction-Induced Faulting

The conditions for the onset of global contraction-induced thrust faulting in a planetary lithosphere are most favorable at or near the surface, as the strength of the lithosphere (Figures 1 and 2), and hence the magnitude of the differential stresses needed to overcome the frictional resistance to sliding on preexisting planes of weakness, are both lowest there [*Klimczak et al.*, 2015]. The near-surface horizontal stresses (σ_H) produced by global contraction of a planet of radius (R) associated with a change in planetary radius (ΔR) may be estimated in their simplest forms [*Melosh and McKinnon*, 1988] by:

$$\sigma_H = \frac{E}{1-\nu}\frac{\Delta R}{R}, \tag{8}$$

where E and ν are the elastic rock properties Young's modulus and Poisson's ratio, respectively. The use of Young's modulus is only appropriate for intact rock, however, and so stresses derived from equation (8) for fractured lithospheric conditions should make use of the deformation modulus instead (see *Klimczak et al.* [2015] for details).

In a tectonic setting where global contraction prevails, the least compressive principal stress acts vertically and is equal to the overburden (i.e., $\sigma_v = \sigma_3 = \rho g z$), and the most compressive stress acts horizontally (i.e., $\sigma_H = \sigma_1$). It follows then that the limits on the brittle strength of a fractured planetary lithosphere that undergoes global contraction can be characterized by setting equation (4) as equal to equation (8), which

Table 2. Uncertainties of Rock-Physical Parameters as Indicated by Their Deviations From Average and the Resultant Maximum Uncertainties for the Radius Change Calculations[a]

	ρ (kg/m^3)	σ_c (MPa)[b]	m_i [c]	E (GPa)[b]	ν[b]	ΔR_i (km)	ΔR_{max} (km)	ΔR_{min} (km)
Mars	3000 ± 200	266 ± 98	25 ± 8	80 ± 20	0.25 ± 0.05	±1.5	±0.4	< ± 0.1
Mercury	3000 ± 200	266 ± 98	25 ± 8	80 ± 20	0.25 ± 0.05	±1.0	±0.4	< ± 0.1
Moon	3000 ± 200	266 ± 98	25 ± 8	80 ± 20	0.25 ± 0.05	±0.8	±0.3	< ± 0.1

[a]Nominal values used for the analysis may not always correspond to the central value of uncertainty.
[b]*Schultz* [1995].
[c]*Hoek and Brown* [1997].

allows for an assessment of the strain (e.g., the change in planetary radius) that the lithosphere can accommodate prior to the onset of global contraction-induced slip along preexisting planes of weakness in the lithosphere.

Given the range of uncertainties of the strength parameters for basaltic and other polycrystalline mafic rock masses discussed in section 2, the radius change calculations were performed with nominal values (Table 1), consistent with the standard numbers for these rock types on Earth, and with a range of reported values [e.g., *Schultz*, 1995; *Hoek and Brown*, 1997] indicated by their deviations from average (Table 2). Compatible with estimates for intact basaltic rocks and rock masses on planetary surfaces [*Schultz*, 1993, 1995], elastic rock properties of $E = 80 \pm 20$ GPa (with a nominal value of 73 GPa) and $\nu = 0.25 \pm 0.05$ were used (Tables 1 and 2). The degree of fracturing of the lithosphere was accounted for in the strength assessment with the appropriate GSI ranges and the corresponding Hoek-Brown parameters (equations (5a)–(5c) and (6a)–(6c)).

Mars, Mercury, and the Moon each host a global population of thrust fault-related landforms that has been linked to global contraction [e.g., *Watters et al.*, 1998, 2010; *Nahm and Schultz*, 2011; *Byrne et al.*, 2014]. These landforms indicate that faulting has occurred on all of these bodies, and so stresses arising from global contraction must have overcome the frictional resistance to sliding within the lithosphere. If their lithospheres were intact, Mars would have experienced a radial decrease (ΔR_i) of 8.1–8.3 ± 1.5 km, Mercury 5.9–6 ± 1.0 km, and the Moon ~4.2 ± 0.8 km in response to global contraction prior to the onset of thrust faulting, for the set of rock-physical parameters listed in Tables (1) and (2). The deviations represent the maximum uncertainties in radial change prior to the initiation of thrust faulting for the ranges of rock-physical parameters (Table 2) used in this analysis (equations (4) and (8)). The given lower bound of the range of the radius decrease is for faulting directly at the surface and the upper value is for conditions at 30 m depth, to explore the effect of a superposed, cohesionless regolith layer. For the Moon, a 30 m thick regolith layer only has a minimal effect on the radius decrease.

Of course, no rock mass on the scale of a lithosphere has ever likely been intact, and so the results given above for intact rock properties are the extreme upper bounds of the amount of global contraction accommodated by each body prior to the onset of thrust faulting. The extents to which the radii of Mars, Mercury, and the Moon could have decreased prior to the formation of thrust faults for the full range of possible degrees of fracturing of their lithospheres (i.e., $7 < \mathrm{GSI} < 100$) using the nominal parameters (Table 1) are visualized in Figure 5. The resistance to frictional sliding of a rock mass exponentially decreases with GSI rating under both surface conditions (Figure 5, solid lines) and for those conditions below a 30 m thick regolith cover (Figure 5, dashed lines). In the latter case, the resistance to frictional sliding decreases at a lower rate than under surface conditions because of the slight increase in rock mass strength from the confining pressure of 30 m of overburden.

For the lower bound of GSI estimated for Mars' lithosphere (i.e., GSI ≈ 35), the planet experienced a radial decrease of 0.2–0.5 ± 0.1 km, whereas for the upper bound (i.e., GSI ≈ 75), the planet must have decreased in radius by as much as 2.0–2.2 ± 0.4 km prior to the formation of thrust faults. The range of GSI values estimated for a lithosphere with rock types present on Mercury and the Moon (i.e., 50–80) require a minimum ΔR of 0.4–0.6 ± 0.1 km and a maximum ΔR of 1.9–2.1 ± 0.4 km for Mercury, and a minimum and maximum ΔR of 0.3 ± 0.1 km and 1.4 ± 0.3 km, respectively, for the Moon prior to the onset of thrust faulting (Figure 5 and Tables 1 and 2). These results indicate that despite the range of uncertainties in strength parameters, all of these bodies must have contracted radially by hundreds to thousands of meters before developing thrust fault-related landforms.

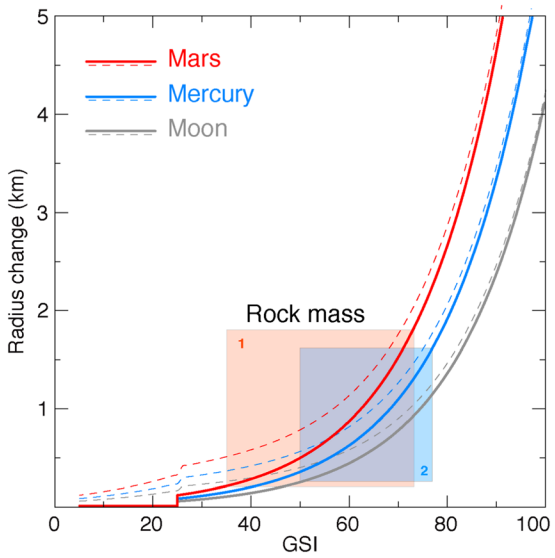

Figure 5. Amounts of radius change of Mars, Mercury, and the Moon at the onset of global contraction-induced faulting for the full range of rock mass qualities. Solid lines represent radius changes with onset of thrust faulting at the surface, while dashed lines show radius changes for faulting below a 30 m thick regolith cover. Typical ranges of rock mass qualities are shown for Mars (red shading) and for Mercury and the Moon (blue shading). See Table 1 for the numerical values of radius changes for each body.

5. Discussion

5.1. Preservation of Strain

The lithospheres of Mars, Mercury, and the Moon are sufficiently strong to have accommodated a considerable amount of radius change from global contraction prior to the onset of thrust faulting. The documented populations of thrust faults on these bodies show that their respective lithospheric compressive strengths were reached, and so strain continued to be accommodated within their lithospheres via frictional sliding. Early studies of faulting reported a weakening effect on lithospheric strength, as coseismic strength drops had been geodetically measured [e.g., *Tsuboi*, 1933, 1956; *Chinnery*, 1964] and slip weakening of shear rupture had been found to occur in brittle strength tests in the laboratory [e.g., *Rummel et al.*, 1978; *Wong*, 1982, 1986; *Li*, 1987]. These findings warrant justification on the state of preservation of strain accommodated by global contraction prior to faulting.

Debate exists on the strength of crustal fault zones (for detailed discussion see *Scholz* [2002]), but increasing evidence shows that the Earth's fractured lithosphere is in equilibrium with the frictional strength of faults that are optimally oriented for slip, with coefficients of friction consistent with a strong lithosphere [*Scholz*, 2002; *Zoback*, 2007]. In particular, a multitude of stress measurements in boreholes and wells point to a strong crust that is in frictional failure equilibrium as predicted by Coulomb theory with friction coefficients of $\mu = 0.6$–1.0 [*Zoback and Healy*, 1984; *Zoback and Harjes*, 1997; *Zoback and Townsend*, 2001]. These values imply stick-slip conditions, where the frictional resistance to sliding of a fault has to be overcome for a slip event to occur. A coefficient of friction value of $\mu = 0.6$ formed the basis for the strength assessment in this study (equations 1–4), and so the resistance to frictional sliding for faults oriented favorably within the tectonic stress field in the fractured lithospheres of Mars, Mercury, and the Moon is captured by all of the failure criteria considered here. In the case where existing faults are not favorably oriented within the tectonic stress field they are not likely to slip [e.g., *Zoback*, 2007]. Instead, a new fault will form, utilizing a favorably oriented preexisting weakness, for which stresses are also required to overcome the frictional resistance to sliding (equations (1), (2), and (4)).

Therefore, the stresses from global contraction within a fractured lithosphere that are required to trigger a slip event are the same irrespective of whether that slip event takes place on a discontinuity for the first time or whether multiple previous slip events already occurred on that discontinuity. Consequently, lithospheres undergoing global contraction that are in frictional failure equilibrium, such as assumed here for the lithospheres on Mars, Mercury, and the Moon, likely preserve any strain accommodated prior to the onset of thrust faulting, if their cohesive properties are not drastically reduced by the faulting events.

Earth, a tectonically active planet with many faults, is not known to have only minimum values for GSI and RMR ratings (e.g., RMR < 8) to drastically reduce cohesive properties and so the strength of assessed volumes of rock. Although the underlying cause of fracturing on Earth differs in nature to that found on the other terrestrial planets, it is undeniable that plenty of faults, fractures, and other discontinuities are present in Earth's lithosphere. The majority of RMR ratings (Figure 3) are far above their minimum possible values, indicating that some degree of cohesion (and thus unconfined compressive strength) is retained on the lithospheric scale despite the presence of multiple sets of fractures and large fault zones.

On the Moon, the scale of the thrust fault-related landforms attributed to have formed as a response to global contraction is relatively small [*Watters et al.*, 2010; *Banks et al.*, 2012; *Williams et al.*, 2013; *Watters et al.*, 2015b]. The amount of radius change that this population of faults accommodated [*Watters et al.*, 2010] is far lower than that determined in this study to have occurred prior to thrust faulting (see section 5.4. for further discussion). This finding indicates that the strain accommodated prior to the onset of thrust faulting must be preserved within the lunar lithosphere.

As the overall frictional and cohesive properties of a lithosphere are not found to be substantially affected by the growth of faults that utilize preexisting planes of weakness, the radius changes accommodated prior to the onset of faulting induced by global contraction are still supported by the lithospheres of Mars, Mercury, and the Moon, even after the formation of thrust faults on each of these bodies. The large spatial and temporal scales of the process of global contraction are likely not comparable to results from regional-scale geophysical monitoring on Earth and laboratory testing. Estimates of planetary radius changes on these bodies reported from thrust fault mapping alone are thus not inclusive of the amount of contraction accommodated prior to the onset of thrust faulting.

5.2. Relevance for Global Contraction on Mars

Thrust fault-related landforms on Mars are found globally, but there are likely several regional populations located in volcanic plains units, impact basins, and the southern highlands [*Knapmeyer et al.*, 2006]. Many of the thrust fault-related landforms, especially the ones in the southern highlands and along the dichotomy boundary, show substantial topography [e.g., *Schultz and Watters*, 2001; *Watters*, 2003], with the faults underlying the landforms reported to penetrate the lithosphere to a depth of 25–30 km [*Schultz and Watters*, 2001]. Fault mapping with 1 km/pixel Mars Orbiter Laser Altimeter data [*Knapmeyer et al.*, 2006], combined with thrust fault displacement analysis [*Watters and Robinson*, 1999; *Watters et al.*, 2000; *Watters*, 2003], showed that Mars may have experienced a decrease in radius of between 0.2 and 3.8 km [*Nahm and Schultz*, 2011].

Uncertainties for radius change estimates accommodated by the thrust faults on Mars result from a combination of the tectonic mapping and the extrapolation of strain analyzed for a few faults to the entire mapped fault population. There is only one detailed global fault map for Mars [*Knapmeyer et al.*, 2006], on which global contraction estimates are based. No uncertainty from the mapping is therefore reflected in the range of estimated radius changes. The bounds for planetary contraction of 0.2 km and 3.8 km reported by *Nahm and Schultz* [2011] only result from different strain estimates for the thrust faults arising from a range of assumed fault population statistics.

From the results of this study, then, the change in radius calculated from thrust fault mapping alone [*Nahm and Schultz*, 2011] underestimated the amount of total global contraction of Mars by as much as 0.2 ± 0.1 to 2.2 ± 0.4 km, with the values of radial change accommodated in the lithosphere prior to thrust faulting being on the same order of magnitude than the estimates from mapped faults. Consequently, the total radius decrease on Mars may be as great as 0.4 to 6.0 km.

Rock mass strength on Mars was assessed for dry conditions in this work, yet liquid water has played an important and long-lasting role in the evolution of the Martian surface and was likely abundant in its lithosphere at the time of deformation. The extent to which water affected the lithospheric strength on Mars must therefore be accounted for with pore pressure evaluations in future analyses.

5.3. Relevance for Global Contraction on Mercury

For Mercury, numerous estimates of radial change resulting from global contraction exist. Since the Mariner 10 spacecraft first imaged the surface of Mercury, revealing large positive-relief landforms that were interpreted to be underlain by thrust faults [*Strom et al.*, 1975], radius changes have been published as new data and techniques became available. First, estimates of the amount of radial contraction were found to range from 1 to 2 km [*Strom et al.*, 1975], with results subsequently updated to amount to less than 1 km [*Watters et al.*, 1998], 0.6 to 0.8 km [*Watters et al.*, 2009], 0.4 to 0.6 km [*Watters and Nimmo*, 2010], and 2.4 to 3.6 km [*Di Achille et al.*, 2012], using Mariner 10 or a combination of Mariner 10 and MErcury Surface, Space ENvironment, GEochemistry, and Ranging (MESSENGER) flyby image data. Several mapped thrust faults on Mercury have been inferred to penetrate the planet's lithosphere to depths of up to 35–40 km [*Watters et al.*, 2002].

Two global thrust fault maps from MESSENGER orbital data have been published to date [*Byrne et al.*, 2014; *Watters et al.*, 2015a]. *Byrne et al.* [2014] report almost 6000 thrust fault-related landforms on Mercury with large-scale tectonic patterns described including fold and thrust belts in excess of 1000 km in length, thrust faults following the rims of large impact basins for hundreds of kilometers, and thrust faults bordering expanses of high-standing terrain. The amount of planetary radius decrease estimated from the mapped population of faults in *Byrne et al.* [2014] was found to range from 3.1 to 7.1 km, with the variance a function once more of assumed fault population statistics. The work presented in *Watters et al.* [2015a] possessed far fewer thrust fault-related landforms than reported by *Byrne et al.* [2014] and did not provide estimates of the amount of global contraction.

As with Mars, the uncertainties for planetary radius change estimates accommodated by the thrust faults on Mercury result from a combination of the tectonic mapping and strain assessment. Although uncertainties from assumptions in thrust fault architecture and their impact on the strain estimates of the global fault population are introduced in each analysis, the large range of reported values of planetary radial change for Mercury from as low as 0.4 km [*Watters et al.*, 2009] to as much as 7.1 km [*Byrne et al.*, 2014] is predominantly from the difference in the number of mapped structures.

Nonetheless, the change in radius calculated from thrust fault mapping does not include the values of radial change accommodated in the lithosphere prior to thrust faulting, which is found in this study to amount to an additional 0.4 ± 0.1 to 2.1 ± 0.4 km. The lower bound of strain accommodated prior to the onset of thrust faulting is approximately equal to the lower value derived from mapping reported by *Watters et al.* [2009], whereas the upper bound exceeds this mapping estimate by as many as five times. Relative to the results by *Di Achille et al.* [2012] and *Byrne et al.* [2014], the strain accommodated prior to the formation of thrust faults is lower but still within 1 order of magnitude of the values reported in these studies.

If Mercury's lithosphere were fractured to a high degree, the amount of contraction needed to overcome the frictional resistance to sliding on planes of weakness would be required to be at least 0.4 ± 0.1 km. However, *Watters et al.* [2015a] regarded Mercury's lithosphere with strength properties derived for RMR values of or below 75 [e.g., *Klimczak et al.*, 2015] as unusually weak. If Mercury's lithosphere were indeed characterized by a low degree of fracturing, it would likely be sufficiently strong so as not to have experienced an onset of thrust faulting until the planet had contracted radially by as much as 2.1 ± 0.4 km. Consequently, the planetary radius decrease accommodated on Mercury prior to the onset of thrust faulting adds substantially to the amount of global contraction reported from mapping studies, which may be anywhere above 2.5 km, but as high as 9.2 km. Of note, even this highest value is well within the maximum permissible value predicted by thermal evolution models [e.g., *Solomon*, 1977].

5.4. Relevance for Global Contraction on the Moon

Thrust fault-related landforms on the Moon are regarded as belonging to one of two distinct populations, the first comprising very small-scale structures that are mainly located in the lunar highlands [*Watters et al.*, 2010; *Banks et al.*, 2012; *Williams et al.*, 2013; *Watters et al.*, 2015b], and the other including many large-scale structures contained within mare units [e.g., *Watters and Johnson*, 2010; *Yue et al.*, 2015]. The landforms that were previously interpreted to have formed from shortening induced by global contraction included only the small-scale structures [*Watters and Johnson*, 2010; *Watters et al.*, 2010, 2015b]. The distribution of this population across the Moon is sparse (see *Watters et al.* [2015b] for a map), and their underlying faults are found to be contained solely within the megaregolith, only penetrating the lunar lithosphere 1 km or less [*Williams et al.*, 2013]. The amount of radius decrease thought to have been accommodated by these faults is estimated to be 0.025 to 0.1 km [*Watters and Johnson*, 2010; *Watters et al.*, 2010, 2015b].

The radius change estimate accommodated by the thrust faults on the Moon is subject to the same uncertainties as presented for Mercury and Mars, as the same approach for the estimation is used [e.g., *Watters and Johnson*, 2010; *Watters et al.*, 2010]. The values of lunar radius decrease derived from structural mapping of 0.025 and 0.1 km reported by *Watters et al.* [2015b] and *Watters et al.* [2010] are up to an order of magnitude lower than the values of contraction prior to the onset of faulting, indicating that the extent to which the lunar structures have accommodated a reduction in the Moon's radius on the basis of thrust fault mapping grossly underestimates the actual amount of radius change of the body. The amount of radius decrease of the Moon likely exceeds 0.3 ± 0.1 to 1.4 ± 0.3 km absent any thrust faulting. This finding reduces the

discrepancy between the observed radius change of 0.025 to 0.1 km [*Watters and Johnson*, 2010; *Watters et al.*, 2010, 2015b] and modeled radius changes in excess of 1 km [e.g., *Solomon and Chaiken*, 1976; *Solomon*, 1977; *Laneuville et al.*, 2013; *Zhang et al.*, 2013] and indicates that future radius change estimates must consider the amount of contraction that was accommodated prior to the formation of the lunar thrust faults.

That the lunar thrust faults interpreted to have been formed by global contraction are found only in the megaregolith [*Williams et al.*, 2013, 2015b] may indicate a partitioning of global contraction-induced strain, with the majority of the lithosphere sufficiently strong to resist frictional sliding and support a radius decrease in a purely elastic manner, and only the much weaker near-surface regolith materials allowing for global contraction-induced fault slip. In addition, the much larger thrust fault-related landforms in mare-filled impact basins [e.g., *Yue et al.*, 2015] on the Moon's nearside are underlain by structures that penetrate the lunar lithosphere to depths of 20 km and that host fault displacements in excess of 1 km [*Byrne et al.*, 2015]. The role that these large structures play for global contraction and how they respond to the Moon's modern-day stress field has been ignored [e.g., *Watters et al.*, 2015b], although their kinematics are reported not to be inconsistent with strain accumulation from global contraction [*Byrne et al.*, 2015]. It may be then that at least some of the strain accommodated by these lithospheric-scale structures might be related to global contraction but is not included in currently published radius change estimates.

5.5. Implications for the Timing and Rate of Global Contraction

The fact that planetary lithospheres undergoing global contraction can accommodate strain prior to the formation of thrust faults has important consequences for the timing and rate of contraction. As strain is found to have been accommodated elastically before the formation of thrust faults, the onset of global contraction must precede the earliest evidence for thrust faulting preserved in the geological records of Mars, Mercury, and the Moon. Furthermore, the amounts of global contraction accommodated before and after the formation of thrust faults and their placement into the geological record provide first-order clues to the rates of contraction on these bodies.

On Mars, the timing of faulting was inferred from the ages of the geologic units in which the faults are found [*Knapmeyer et al.*, 2006]. A small portion of thrust fault-related landforms was mapped in Early Noachian units and so they were classified as 3.95–3.99 Ga [*Knapmeyer et al.*, 2006]. As this methodology determines the earliest possible ages of slip events within the geologic units in which the faults have surface expressions, it does not fully characterize the onset of faulting or the time span of deformation. Faulting may have been initiated much later or activity might have lasted beyond the specific time periods to which each fault was assigned. Nevertheless, if thrust faulting in this part of Mars occurred at 3.95–3.99 Ga, then 0.2 ± 0.1 to 2.2 ± 0.4 km of radial contraction was accommodated in the lithosphere prior to this model age [*Knapmeyer et al.*, 2006], indicating that global contraction on Mars began without any surface manifestation at or somewhat prior to the end of the late heavy bombardment.

Thermal history models for Mars predict an increased rate for the accumulation of contractional strain prior to 3.7 Ga [*Andrews-Hanna et al.*, 2008]. *Nahm and Schultz* [2011] found that ~59% of total global contractional strain was accommodated by thrust faults between 3.8 and 3.6 Ga, but they argued against an increased rate of global contraction in that time interval and attributed most of the faulting to regional-scale processes. However, higher strain rates in the early history of Mars are required for the entire range of radial changes that occurred prior to the onset of thrust faulting if thrust faults on Mars accommodated only 0.2 km of radial contraction after 3.6 to 4 Ga. Higher initial strain rates on Mars are also required to accommodate 2.2 km of radial contraction prior to the initiation of thrust faulting at 3.6 to 4 Ga if the thrust faults accommodated 3.8 km of radial contraction. Higher strain rates in Mars' early geologic history are not inconsistent with, but are not necessary for, the scenario under which the planet experienced 3.8 km of radial contraction accommodated by the thrust faults after 3.6 to 4 Ga, but contracted by only 0.2 km before the onset of thrust faulting. These findings indicate that the rate at which global contraction operated on Mars was probably not constant.

On Mercury, the timing of thrust faulting was inferred from relationships with impact craters of different degradation stages [*Banks et al.*, 2015]. Thrust faults superposed by craters, whose degradation stage is consistent with their formation in the Calorian period, confine the earliest fault activity to ~3.9 to ~3.5 Ga [*Spudis and Guest*, 1988]. Similar to findings for Mars, such a timing relationship for Mercury implies that the onset of global contraction accounting for the strain accommodated prior to the formation of thrust

faults took place at or somewhat before the end of the late heavy bombardment with no manifestation in the geological record.

Thermal history models for Mercury predict an initial phase of interior heating and planetary expansion, followed by secular cooling that frequently result in an approximately constant rate of radial decrease [e.g., *Solomon*, 1977; *Michel et al.*, 2013; *Tosi et al.*, 2013]. But as for Mars, higher strain rates in Mercury's early geologic history, i.e., prior to ~3.9 to ~3.5 Ga, are consistent with all combinations of planetary radius changes that were accommodated before and after the onset of thrust faulting. Only the end-member scenario, under which Mercury accommodated 5 to 7 km of radius change by thrust faulting [*Byrne et al.*, 2014] but only experienced a reduction in radius of 0.4 km prior to the formation of the thrust faults, does not require a higher rate of global contraction in the early history of the planet. These findings indicate that similar to results for Mars, there is a high probability that the rate at which global contraction operated on Mercury has decreased over time.

For the Moon, the onset and timing of global contraction-induced thrust faulting is unclear. Based on crosscutting relationships with small craters, the population of small landforms attributed to global contraction was inferred to be younger than 1 Ga [*Watters et al.*, 2010], whereas thermal history models require that contraction began at or before ~3.6 Ga [e.g., *Laneuville et al.*, 2013; *Zhang et al.*, 2013]. The role of preservation of the surface expressions of the small thrust faults over geologic time, as well as a potential contribution to global contraction of the larger thrust faults deforming the lunar mare units [*Byrne et al.*, 2015], remain largely unexplored. Both of these factors, however, are key for a better understanding of the timing and amount of radial changes accommodated by the thrust faults on the Moon.

5.6. Global Contraction and the Late Heavy Bombardment

Resurfacing from impact cratering and basin formation has the potential to erase tectonic landforms, and so it has been assumed that some amount of radial change would not be preserved in the geologic record if the onset of global contraction overlapped with the late heavy bombardment [e.g., *Hauck et al.*, 2004; *Watters et al.*, 2009]. Indeed, a basin-forming impact event, such as that producing the Caloris basin on Mercury, was probably accompanied by heating and melting in the near-surface, likely resetting preexisting stresses from global contraction and producing melts that lead to volcanism and so to the production of new crustal material at and near the impact site [*Roberts and Barnouin*, 2012]. Such process would indeed erase any preexisting landforms at the site of impact if they were present at the time of basin formation. Smaller impacts would also superpose and so cover preexisting structures directly at the impact site. However, impact-related processes likely do not erase the amount of contraction accommodated in a fractured lithosphere prior to the onset of thrust faulting (Table 1), as essentially new lithosphere from basin-forming events is subject to the same limits of brittle strength for the onset of thrust faulting as outlined in section 2, irrespective of the causes and degree of fracturing. The weakening effect of impact damage surrounding large basins, as accounted for by using strength properties of rock masses for a range of degrees of fracturing, might favor an earlier onset of thrust faulting around large basins.

If global contraction operated early in the geologic histories of Mars, Mercury, and the Moon, a heavy impact bombardment and widespread basin formation with multiple overlapping basins would have the potential to delay the accommodation of strain, and so the onset of thrust faulting at the impact sites. After the impact, the lithosphere would have to be newly formed and sufficiently cooled to below the elastic blocking temperature [e.g., *Turcotte*, 1983], and stresses generated by global contraction would have to build up to reach the critical value for frictional sliding to occur. It follows that a multitude of large basin-forming events early in the geologic history of a rocky planet might not allow for the accommodation of strain from global contraction at the same time. Therefore, the onset of strain accommodation prior to and by frictional sliding induced by global contraction on Mars, Mercury, and the Moon is unlikely to have occurred much earlier than the end of the late heavy bombardment.

6. Conclusions

The lithospheres of planets are neither fully intact nor do they completely lack cohesion. Instead, they consist of a rock mass composed of small to large blocky, interlocked rock fragments, lowering the cohesive properties of the rock volume but not reducing them entirely to zero. The degree of rock mass fragmentation and

fracturing is characterized with the Rock Mass Rating System (RMR) or the Geologic Strength Index (GSI), which can then be utilized to assess the lithospheric strength on scales at which rocks are no longer intact. Application to the study of global contraction of Mars, Mercury, and the Moon shows that these bodies' lithospheres are strong enough to support some amount of stress, and hence accommodate strain, prior to the formation of thrust faults, with the amount of accommodated strain dependent on the extent of lithospheric fracturing.

That lithospheres can take up some portion of strain prior to the onset of faulting is not surprising, but has not been considered in the context of global contraction before. This finding adds a new component to the study of global contraction in terms of the amount, timing, and rate of radius change on Mars, Mercury, and the Moon. It increases the estimates for planetary radius changes on these bodies, a result most relevant for understanding the global contraction of the Moon, which may have accommodated a change in radius of more than 50 times that estimated from thrust fault mapping alone. That lithospheres can accommodate strain prior to the onset of brittle failure also implies that the start of global contraction predates the temporal evidence preserved in the geologic record, which on Mars and Mercury may have been as early as the end of the late heavy bombardment. Moreover, the results given here that pertain to the amount and timing of strain accommodation indicate that the rates with which global contraction operated were higher in the early geologic histories of Mars and Mercury. Together, these findings give a more comprehensive insight into the study of global contraction of planetary bodies, and so are as relevant for geologists reporting observations from tectonic mapping as for geophysicists modeling thermal histories of planetary bodies.

Acknowledgments

The author thanks Paul K. Byrne and Steven A. Hauck, II for their edits and suggestions on several versions of this paper. This paper also benefitted from reviews by Laurent Montesi and an anonymous reviewer. This research was in part funded by NASA's MDAP program under award NNX14AR89G. The methods and data used to produce the results of this paper are freely available in the published literature.

References

Ahrens, T. J., and A. M. Rubin (1993), Impact-induced tensional failure in rock, *J. Geophys. Res.*, *98*(E1), 1185–1203, doi:10.1029/92JE02679.

Anderson, E. M. (1951), *The Dynamics of Faulting and Dyke Formation, With Applications to Britain*, Oliver and Boyd, Edinburgh.

Andrews-Hanna, J. C., M. T. Zuber, and S. A. Hauck II (2008), Strike-slip faults on Mars: Observations and global implications for tectonics and geodynamics, *J. Geophys. Res.*, *113*, E08002, doi:10.1029/2007JE002980.

Banks, M. E., T. R. Watters, M. S. Robinson, L. L. Tornabene, T. Tran, L. Ojha, and N. R. Williams (2012), Morphometric analysis of small-scale lobate scarps on the Moon using data from the Lunar Reconnaissance Orbiter, *J. Geophys. Res.*, *117*, E00H11, doi:10.1029/2011JE003907.

Banks, M. E., Z. Xiao, T. R. Watters, R. G. Strom, S. E. Braden, C. R. Chapman, S. C. Solomon, C. Klimczak, and P. K. Byrne (2015), Duration of activity on lobate-scarp thrust faults on Mercury, *J. Geophys. Res. Planets*, *120*, doi:10.1029/2015JE004828.

Bieniawski, Z. T. (1973), Engineering classification of jointed rock masses, *Trans. S. Afr. Inst. Civil Eng.*, *15*, 335–344.

Bieniawski, Z. T. (1976), Rock mass classification in rock engineering, in *Exploration for Rock Engineering*, *Proc. Symp*, vol. 1, edited by Z. T. Bieniawski, pp. 97–106, Balkema, Cape Town.

Bieniawski, Z. T. (1989), *Engineering Rock Mass Classifications*, 251 pp., Wiley, New York.

Brace, W. F., and D. L. Kohlstedt (1980), Limits on lithospheric stress imposed by laboratory experiments, *J. Geophys. Res.*, *85*(B11), 6248–6252, doi:10.1029/JB085iB11p06248.

Byerlee, J. D. (1967a), Frictional characteristics of granite under high confining pressure, *J. Geophys. Res.*, *72*, 3639–3648, doi:10.1029/JZ072i014p03639.

Byerlee, J. D. (1967b), Theory of friction based on brittle failure, *J. Appl. Phys.*, *38*, 2928–2934.

Byerlee, J. D. (1978), Friction of rocks, *Pure Appl. Geophys.*, *116*(4–5), 615–626, doi:10.1007/BF00876528.

Byrne, P. K., C. Klimczak, A. M. C. Şengör, S. C. Solomon, T. R. Watters, and S. A. Hauck II (2014), Mercury's global contraction much greater than earlier estimates, *Nat. Geosci.*, *7*(4), 301–307, doi:10.1038/ngeo2097.

Byrne, P. K., C. Klimczak, P. J. McGovern, E. Mazarico, P. B. James, G. A. Neumann, M. T. Zuber, and S. C. Solomon (2015), Deep-seated reverse faults bound the Mare Crisium mascon, *Earth Planet. Sci. Lett.*, *427*, 183–190, doi:10.1016/j.epsl.2015.06.022.

Carrier, W. D., III, G. R. Olhoeft, and W. Mendell (1991), Physical properties of the lunar surface, in *Lunar Sourcebook: A User's Guide to the Moon*, edited by G. H. Heiken, G. D. Vaniman, and B. M. French, pp. 475–594, Cambridge Univ. Press, New York.

Chinnery, M. A. (1964), The strength of the Earth's crust under horizontal shear stress, *J. Geophys. Res.*, *69*, 2085–2089, doi:10.1029/JZ069i010p02085.

Collins, G. S., H. J. Melosh, and B. A. Ivanov (2004), Modeling damage and deformation in impact simulations, *Meteorit. Planet. Sci.*, *39*(2), 217–231, doi:10.1111/j.1945-5100.2004.tb00337.x.

Dainty, A. M., M. N. Toksöz, K. R. Anderson, P. J. Pines, Y. Nakamura, and G. Latham (1974), Seismic scattering and shallow structure of the moon in Oceanus Procellarum, *Moon*, *9*(1–2), 11–29, doi:10.1007/BF00565388.

Di Achille, G., C. Popa, M. Massironi, E. M. Epifani, M. Zusi, G. Cremonese, and P. Palumbo (2012), Mercury's radius change estimates revisited using MESSENGER data, *Icarus*, *221*(1), 456–460, doi:10.1016/j.icarus.2012.07.005.

Dombard, A. J., and S. A. Hauck II (2008), Despinning plus global contraction and the orientation of lobate scarps on Mercury: Predictions for MESSENGER, *Icarus*, *198*(1), 274–276, doi:10.1016/j.icarus.2008.06.008.

Emmermann, R., and J. Lauterjung (1997), The German Continental Deep Drilling Program KTB: Overview and major results, *J. Geophys. Res.*, *102*(B8), 18,179–18,201, doi:10.1029/96JB03945.

Goodman, R. E. (1989), *Introduction to Rock Mechanics*, 2nd ed., 562 pp., Wiley, New York.

Haskin, L. A., et al. (2005), Water alteration of rocks and soils on Mars at the Spirit rover site in Gusev crater, *Nature*, *436*(7047), 66–69, doi:10.1038/nature03640.

Hauck, S. A., II, and R. J. Phillips (2002), Thermal and crustal evolution of Mars, *J. Geophys. Res.*, *107*(E7), 5052, doi:10.1029/2001JE001801.

Hauck, S. A., II, A. J. Dombard, R. J. Phillips, and S. C. Solomon (2004), Internal and tectonic evolution of Mercury, *Earth Planet. Sci. Lett.*, *222*(3–4), 713–728, doi:10.1016/j.epsl.2004.03.037.

Hoek, E. (1994), Strength of rock and rock masses, *Int. Soc. Rock Mech. News J.*, *2*(2), 4–16.

Hoek, E., and E. T. Brown (1980), Empirical strength criterion for rock masses, *ASCE J. Geotech. Eng. Div.*, *106*, 1013–1035.
Hoek, E., and E. T. Brown (1988), The Hoek-Brown failure criterion—A 1988 update, Proceedings of the 15th Canadian Rock Mechanics Symposium.
Hoek, E., and E. T. Brown (1997), Practical estimates of rock mass strength, *Int. J. Rock Mech. Min. Sci.*, *34*(8), 1165–1186, doi:10.1016/S1365-1609(97)80069-X.
Hoek, E., D. Wood, and S. Shah (1992), A modified Hoek-Brown criterion for jointed rock masses, in *Proceedings of the International Society for Rock Mechanics Symposium on Rock Characterization*, edited by J. A. Hudson, pp. 209–214, Brit. Geol. Soc, Chester, U. K.
Jaeger, J. C., N. G. W. Cook, and R. W. Zimmerman (2007), *Fundamentals of Rock Mechanics*, 4th ed., 575 pp., Wiley Blackwell, Malden, Mass.
Klimczak, C. (2014), Geomorphology of lunar grabens requires igneous dikes at depth, *Geology*, *42*, 963–966, doi:10.1130/G35984.1.
Klimczak, C., P. K. Byrne, and S. C. Solomon (2015), A rock-mechanical assessment of Mercury's global tectonic fabric, *Earth Planet. Sci. Lett.*, *416*, 82–90, doi:10.1016/j.epsl.2015.02.003.
Knapmeyer, M., J. Oberst, E. Hauber, M. Wählisch, C. Deuchler, and R. Wagner (2006), Working models for spatial distribution and level of Mars' seismicity, *J. Geophys. Res.*, *111*, E11006, doi:10.1029/2006JE002708.
Kohlstedt, D. L., and S. J. Mackwell (2010), Strength and deformation of planetary lithospheres, in *Planetary Tectonics*, edited by T. R. Watters and R. A. Schultz, pp. 397–456, Cambridge Univ. Press, New York.
Laneuville, M., M. A. Wieczorek, D. Breuer, and N. Tosi (2013), Asymmetric thermal evolution of the Moon, *J. Geophys. Res. Planets*, *118*, 1435–1452, doi:10.1002/jgre.20103.
Li, V. C. (1987), Mechanics of shear rupture applied to earthquake zones, in *Fracture Mechanics of Rock*, edited by B. K. Atkinson, pp. 351–428, Acad. Press Inc. LTD, London, U. K.
Lin, L., H. Jia, and Y. Xu (2007), Fracture network characteristics of a deep borehole in the Table Mountain Group (TMG), South Africa, *Hydrogeol. J.*, *15*(7), 1419–1432, doi:10.1007/s10040-007-0184-y.
Marinos, P., and E. Hoek (2000), GSI: A geologically friendly tool for rock mass strength estimation, in *Proceedings of the GeoEng2000 at the International Conference on Geotechnical and Geological Engineering*, pp. 1446–1422, Tech. Publ., Lancaster, Melbourne.
Melosh, H. J. (1984), Impact ejection, spallation, and the origin of meteorites, *Icarus*, *59*(2), 234–260, doi:10.1016/0019-1035(84)90026-5.
Melosh, H. J., and W. B. McKinnon (1988), The tectonics of Mercury, in *Mercury*, edited by F. Vilas, C. R. Chapman, and M. S. Matthews, pp. 374–428, Univ. Ariz. Press, Tuscon, Ariz.
Michel, N. C., S. A. Hauck II, S. C. Solomon, R. J. Phillips, J. H. Roberts, and M. T. Zuber (2013), Thermal evolution of Mercury as constrained by MESSENGER observations, *J. Geophys. Res. Planets*, *118*, 1033–1044, doi:10.1002/jgre.20049.
Nahm, A. L., and R. A. Schultz (2007), Outcrop-scale physical properties of Burns Formation at Meridiani Planum, Mars, *Geophys. Res. Lett.*, *34*, L20203, doi:10.1029/2007GL031005.
Nahm, A. L., and R. A. Schultz (2011), Magnitude of global contraction on Mars from analysis of surface faults: Implications for Martian thermal history, *Icarus*, *211*(1), 389–400, doi:10.1016/j.icarus.2010.11.003.
Roberts, J. H., and O. S. Barnouin (2012), The effect of the Caloris impact on the mantle dynamics and volcanism of Mercury, *J. Geophys. Res.*, *117*, E02007, doi:10.1029/2011JE003876.
Rummel, F., H. J. Alheid, and C. Frohn (1978), Dilatancy and fracture induced velocity changes in rock and their relation to frictional sliding, *Pure Appl. Geophys.*, *116*, 743–764.
Scholz, C. H. (2002), *The Mechanics of Earthquakes and Faulting*, 471 pp., Cambridge Univ. Press, Cambridge.
Schubert, T. S., and T. Spohn (1990), Thermal history of Mars and the sulfur content of its core, *J. Geophys. Res.*, *95*(B9), 14,095–14,104, doi:10.1029/JB095iB09p14095.
Schultz, R. A. (1992a), Limitations on the applicability of Byerlee's law and the Griffith criterion to shallow crustal conditions, 23rd Lunar and Planetary Science Conference, 1239, Houston, Tex.
Schultz, R. A. (1992b), What's the difference between a rock and a rock mass (and why is it important?), 23rd Lunar and Planetary Science Conference, #1243, Houston, Tex., U.S.A.
Schultz, R. A. (1993), Brittle strength of basaltic rock masses with applications to Venus, *J. Geophys. Res.*, *98*(E6), 10,883–10,895, doi:10.1029/93JE00691.
Schultz, R. A. (1995), Limits on strength and deformation properties of jointed basaltic rock masses, *Rock Mech. Rock Eng.*, *28*(1), 1–15, doi:10.1007/BF01024770.
Schultz, R. A. (1996), Relative scale and the strength and deformability of rock masses, *J. Struct. Geol.*, *18*(9), 1139–1149.
Schultz, R. A., and H. Fossen (2008), Terminology for structural discontinuities, *AAPG Bull.*, *92*(7), 853–867, doi:10.1306/02200807065.
Schultz, R. A., and T. R. Watters (2001), Forward mechanical modeling of the Amenthes Rupes thrust fault on Mars, *Geophys. Res.Lett.*, *28*(24), 4659–4662, doi:10.1029/2001GL013468.
Schultz, R. A., C. H. Okubo, and S. J. Wilkins (2006), Displacement-length scaling relations for faults on the terrestrial planets, *J. Struct. Geol.*, *28*(12), 2182–2193, doi:10.1016/j.jsg.2006.03.034.
Seeburger, D. A., and M. D. Zoback (1982), The distribution of natural fractures and joints at depth in crystalline rock, *J. Geophys. Res.*, *87*(B7), 5517–5534, doi:10.1029/JB087iB07p05517.
Serafim, J. L., and J. P. Pereira (1983), Consideration of the geomechanical classification of Bieniawski, Proc. Int. Symp. Eng. Geol. Underground Constr. Lisbon, 1(II), 33–44.
Shearer, C. K., et al. (2006), Thermal and Magmatic Evolution of the Moon, edited by W. K. Hartmann, R. J. Phillips and G. J. Taylor, *Rev. Mineral. Geochem.*, *60*(1), 365–518, doi:10.2138/rmg.2006.60.4.
Snow, D. T. (1968), Rock fracture spacings, openings, and porosities, *ASCE J. Soil Mech. Found. Div.*, *94*(1), 73–92.
Solomon, S. C. (1977), The relationship between crustal tectonics and internal evolution in the Moon and Mercury, *Phys. Earth Planet. Inter.*, doi:10.1016/0031-9201(77)90026-7.
Solomon, S. C. (1986), On the early thermal state of the Moon, in *Origin of the Moon*, pp. 435–452, Lunar and Planet. Inst., Houston, Tex.
Solomon, S. C., and J. Chaiken (1976), Thermal expansion and thermal stress in the Moon and terrestrial planets: Clues to early thermal history, *Proc. Lunar Planet.Sci. Conf.*, *7*, 3229–3243.
Spudis, P. D., and J. E. Guest (1988), Stratigraphy and geologic history of Mercury, in *Mercury*, edited by F. Vilas, C. R. Chapman, and M. S. Matthews, pp. 118–164, Univ. Ariz. Press, Tucson, Ariz.
Strom, R. G., N. J. Trask, and J. E. Guest (1975), Tectonism and volcanism on Mercury, *J. Geophys. Res.*, *80*(17), 2478–2507, doi:10.1029/JB080i017p02478.
Thomson, B. J., N. T. Bridges, J. Cohen, J. A. Hurowitz, A. Lennon, G. Paulsen, and K. Zacny (2013), Estimating rock compressive strength from Rock Abrasion Tool (RAT) grinds, *J. Geophys. Res. Planets*, *118*, 1233–1244, doi:10.1002/jgre.20061.
Toksöz, M. N., A. M. Dainty, S. C. Solomon, and K. R. Anderson (1974), Structure of the Moon, *Rev. Geophys. Space Phys.*, *12*(4), 539–567, doi:10.1029/RG012i004p00539.

Tosi, N., M. Grott, A. C. Plesa, and D. Breuer (2013), Thermochemical evolution of Mercury's interior, *J. Geophys. Res. Planets*, *118*, 2474–2487, doi:10.1002/jgre.20168.
Tsuboi, C. (1933), Investigation of deformation of the crust found by precise geodetic means, *Jpn.J.Astron. Geophys.*, *10*, 93–248.
Tsuboi, C. (1956), Earthquake energy, earthquake volume, aftershock area, and strength of the Earth's crust, *J. Phys. Earth*, *4*, 63–66.
Turcotte, D. L. (1983), Thermal stresses in planetary elastic lithospheres, *J. Geophys. Res.*, *88*, A585–A587, doi:10.1029/JB088iS02p0A585.
Watters, T. R. (2003), Thrust faults along the dichotomy boundary in the eastern hemisphere of Mars, *J. Geophys. Res.*, *108*(E6), 5054, doi:10.1029/2002JE001934.
Watters, T. R., and C. L. Johnson (2010), Lunar tectonics, in *Planetary Tectonics* edited by Watters, T. R., and R. A. Schultz, pp. 121–182, Cambridge Univ. Press, New York.
Watters, T. R., and F. Nimmo (2010), The tectonics of Mercury, in *Planetary Tectonics* edited by Watters, T. R., and R. A. Schultz, pp. 15–80, Cambridge Univ. Press, New York.
Watters, T. R., and M. S. Robinson (1999), Lobate scarps and the Martian crustal dichotomy, *J. Geophys. Res.*, *104*(E8), 18,981–18,990, doi:10.1029/1998JE001007.
Watters, T. R., M. S. Robinson, and A. C. Cook (1998), Topography of lobate scarps on Mercury: New constraints on the planet's contraction, *Geology*, *26*(11), 991–994.
Watters, T. R., R. A. Schultz, and M. S. Robinson (2000), Displacement-length relations of thrust faults associated with lobate scarps on Mercury and Mars: Comparison with terrestrial faults, *Geophys. Res. Lett.*, *27*(22), 3659–3662, doi:10.1029/2000GL011554.
Watters, T. R., R. A. Schultz, M. S. Robinson, and A. C. Cook (2002), The mechanical and thermal structure of Mercury's early lithosphere, *Geophys. Res. Lett,*, *29*(11), 1542, doi:10.1029/2001GL014308.
Watters, T. R., S. C. Solomon, M. S. Robinson, J. W. Head, S. L. André, S. A. Hauck II, and S. L. Murchie (2009), The tectonics of Mercury: The view after MESSENGER's first flyby, *Earth Planet. Sci. Lett.*, *285*(3–4), 283–296, doi:10.1016/j.epsl.2009.01.025.
Watters, T. R., et al. (2010), Evidence of recent thrust faulting on the Moon revealed by the lunar reconnaissance orbiter camera, *Science*, *329*(5994), 936–940, doi:10.1126/science.1189590.
Watters, T. R., M. M. Selvans, M. E. Banks, S. A. Hauck II, K. J. Becker, and M. S. Robinson (2015a), Distribution of large-scale contractional tectonic landforms on Mercury: Implications for the origin of global stresses, *Geophys. Res. Lett,*, *42*, 3755–3763, doi:10.1002/2015GL063570.
Watters, T. R., M. S. Robinson, G. C. Collins, M. E. Banks, K. Daud, N. R. Williams, and M. M. Selvans (2015b), Global thrust faulting on the Moon and the influence of tidal stresses, *Geology*, *43*(10), 851–854, doi:10.1130/G37120.1.
Wieczorek, M. A., et al. (2013), The crust of the Moon as seen by GRAIL, *Science*, *339*(6120), 671–675, doi:10.1126/science.1231530.
Williams, N. R., T. R. Watters, M. E. Pritchard, M. E. Banks, and J. F. Bell III (2013), Fault dislocation modeled structure of lobate scarps from Lunar Reconnaissance Orbiter Camera digital terrain models, *J. Geophys. Res. Planets*, *118*, 224–233, doi:10.1002/jgre.20051.
Wong, T.-F. (1982), Effects of temperature and pressure on failure and post-failure behavior of Westerly granite, *Mech. Mater.*, *1*, 3–17.
Wong, T.-F. (1986), On the normal stress dependence of the shear fracture energy, in *Earthquake Source Mechanics*, *Geophys. Monogr. 31, Maurice Ewing*, vol. 6, edited by S. Das, J. Boatwright, and C. H. Scholz, pp. 1–12, AGU, Washington, D. C.
Xia, K., and T. J. Ahrens (2001), Impact induced damage beneath craters, *Geophys. Res. Lett,*, *28*(18), 3525–3527, doi:10.1029/2001GL013001.
Yue, Z., W. Li, K. Di, Z. Liu, and J. Liu (2015), Global mapping and analysis of lunar wrinkle ridges, *J. Geophys. Res. Planets*, *120*, 978–994, doi:10.1002/2014JE004777.
Zhang, N., E. M. Parmentier, and Y. Liang (2013), A 3-D numerical study of the thermal evolution of the Moon after cumulate mantle overturn: The importance of rheology and core solidification, *J. Geophys. Res. Planets*, *118*, 1789–1805, doi:10.1002/jgre.20121.
Zoback, M. D. (2007), *Reservoir Geomechanics*, 449 pp., Cambridge Univ. Press, New York.
Zoback, M. D., and H. P. Harjes (1997), Injection induced earthquakes and crustal stress at 9 km depth at the KTB drilling site, Germany, *J. Geophys. Res.*, *102*, 18,477–18,491, doi:10.1002/jgre.20121.
Zoback, M. D., and J. H. Healy (1984), Friction, faulting, and "in situ" stresses, *Ann. Geophys.*, *2*, 689–698.
Zoback, M. D., and J. Townsend (2001), Implications of hydrostatic pore pressures and high crustal strength for the deformation of intraplate lithosphere, *Tectonophysics*, *336*, 19–30.
Zuber, M. T. (2000), Internal structure and early thermal evolution of Mars from Mars Global Surveyor topography and gravity, *Science*, *287*(5459), 1788–1793, doi:10.1126/science.287.5459.1788.